

# Comparison of Gadolinium Concentrations within Multiple Rat Organs after Intravenous Administration of Linear versus Macrocyclic Gadolinium Chelates<sup>1</sup>

Robert J. McDonald, MD, PhD  
 Jennifer S. McDonald, PhD  
 Daying Dai, MD, PhD  
 Dana Schroeder, BS  
 Mark E. Jentoft, MD  
 David L. Murray, MD, PhD  
 Ramanathan Kadirvel, PhD  
 Laurence J. Eckel, MD  
 David F. Kallmes, MD

## Purpose:

To compare gadolinium tissue concentrations of multiple linear and macrocyclic chelates in a rat model to better understand the scope and extent of tissue deposition following multiple intravenous doses of gadolinium-based contrast agent (GBCA).

## Materials and Methods:

In this Institutional Animal Care and Use Committee-approved study, healthy rats received 20 intravenous injections of 2.5 mmol gadolinium per kilogram (gadolinium-exposed group) or saline (control group) over a 26-day period. Unenhanced T1 signal intensities of the dentate nucleus were measured from magnetic resonance (MR) images obtained prior to GBCA injection and 3 days after final injection. Rat brain and renal, hepatic, and splenic tissues were harvested 7 days after final injection and subjected to inductively coupled plasma mass spectrometry and transmission electron microscopy for quantification and characterization of gadolinium deposits.

## Results:

Gadolinium deposition in brain tissue significantly varied with GBCA type ( $F = 31.2$ ;  $P < .0001$ ), with median concentrations of 0  $\mu\text{g}$  gadolinium per gram of tissue (95% confidence interval [CI]: 0, 0.2) in gadoteridol-injected rats, 1.6  $\mu\text{g}$  gadolinium per gram of tissue (95% CI: 0.9, 4.7) in gadobutrol-injected rats, 4.7  $\mu\text{g}$  gadolinium per gram of tissue (95% CI: 3.5, 6.1) in gadobenate dimeglumine-injected rats, and 6.9  $\mu\text{g}$  gadolinium per gram of tissue (95% CI: 6.2, 7.0) in gadodiamide-injected rats; a significant positive dose-signal intensity correlation was identified ( $\rho = 0.93$ ;  $P < .0001$ ). No detectable neural tissue deposition or MR imaging signal was observed in control rats ( $n = 6$ ). Similar relative differences in gadolinium deposition were observed in renal, hepatic, and splenic tissues at much higher tissue concentrations ( $P < .0001$ ). Gadolinium deposits were visualized directly in the endothelial capillary walls and neural interstitium in GBCA-injected rats, but not in control rats.

## Conclusion:

Tissue deposition of gadolinium was two- to fourfold higher following administration of the linear agents gadodiamide and gadobenate dimeglumine compared with the macrocyclic agents gadobutrol and gadoteridol. These findings suggest that organ tissue deposition is reduced but not eliminated following administration of macrocyclic GBCA chelates in lieu of linear chelates.

©RSNA, 2017

Online supplemental material is available for this article.

<sup>1</sup>From the Departments of Radiology (R.J.M., J.S.M., D.D., D.S., R.K., L.J.E., D.F.K.), Laboratory Medicine and Pathology (M.E.J., D.L.M.), and Neurosurgery (D.F.K.), College of Medicine, Mayo Clinic, 200 1st St SW, Rochester, MN 55905. Received July 8, 2016; revision requested September 1; revision received March 8, 2017; accepted March 20; final version accepted March 24. **Address correspondence to R.J.M.** (e-mail: [mcdonald.robert@mayo.edu](mailto:mcdonald.robert@mayo.edu)).

Recent human and animal model studies have revealed the presence of gadolinium deposits in various central nervous system structures following repeated administration of intravenous gadolinium-based contrast agents (GBCAs) (1–6). These studies demonstrated a strongly positive

dose-dependent relationship with tissue concentration based on cumulative lifetime GBCA dose. Such deposition appears to occur in the absence of renal or hepatobiliary dysfunction and, based on limited data, is durable with deposits remaining years after administration of GBCAs. Although the toxicity of GBCAs is low in their chelated form, concern exists that such gadolinium deposits represent a free (dechelated) form, which is of concern given the cytotoxic effects of free gadolinium (7,8). These findings prompted the U.S. Food and Drug Administration and European Medicines Agency to issue safety warnings in 2015 and 2016, respectively, with the intent to more closely examine the risks and biologic effects of these deposits (9,10).

Following these initial reports, Radbruch et al and Kanda et al published imaging evidence that this deposition is limited to linear GBCA chelates and is not observed with macrocyclic GBCAs (11–14). Differences in deposition propensity between GBCA classes have been attributed to the higher intrinsic stability and gadolinium-binding affinity of macrocyclic agents compared with linear agents. Similar mechanistic interpretations have been used to explain the higher incidence of nephrogenic systemic fibrosis following administration of linear agents compared with macrocyclic agents. To date, the

mechanistic understanding of nephrogenic systemic fibrosis and gadolinium deposition in neural tissues remains relatively undefined. Further, it remains unclear if chelate stability alone accounts for the relative differences in deposition observed in humans and animal models.

In the current study, we compared elemental gadolinium tissue concentrations of multiple linear and macrocyclic chelates in a rat model to better understand the scope and extent of tissue deposition following multiple intravenous GBCA doses.

### Advances in Knowledge

- Elemental gadolinium accumulates in murine neural, hepatic, splenic, and renal tissues following intravenous administration of gadolinium-based contrast agent (GBCA).
- Tissue gadolinium concentrations as determined by inductively coupled plasma mass spectrometry demonstrated significant differences in tissue concentrations between linear and macrocyclic GBCAs in all studied tissues in descending order as follows: gadodiamide, gadobenate dimeglumine, gadobutrol, and gadoteridol in a trend that largely parallels the thermodynamic stability constants of these agents.
- Tissue deposition was substantially lower in neural tissues than in hepatic, splenic, and renal tissues with fenestrated capillary systems; notwithstanding, all agents demonstrated some amount of neural tissue deposition ranging from 0.1 to 7  $\mu\text{g}$  gadolinium per gram of tissue.
- Transmission electron microscopy revealed the presence of gadolinium deposits in both endothelial walls, with a smaller fraction of deposits in the interstitium and cells of the dentate nucleus.
- Although no tissue injury was observed in neural, hepatic, and splenic tissues, significant renal injury following GBCA administration was observed and was most extensive in gadoteridol-treated rats in which there was evidence of irreversible tissue injury.

### Implications for Patient Care

- Neuronal tissue deposition of gadolinium appears to take place with both macrocyclic and linear GBCAs, albeit at lower concentrations than with macrocyclic agents.
- Gadolinium deposition is substantially higher in nonneural tissues; some of these tissues may act as a long-term biologic reservoir.
- At high doses, all GBCAs appear to have varying degrees of nephrotoxicity.
- The clinical significance of gadolinium deposition in neural, hepatic, and splenic issues remains poorly understood.

### Materials and Methods

Design and execution of this single-center retrospective study from August 2015 to December 2015 was subject to Institutional Animal Care and Use Committee oversight.

### Study Design and Animals

Healthy male Wistar rats (Charles River Laboratories, Wilmington, Mass) were treated with either intravenous injections of GBCA or saline to assess the extent and significance of gadolinium deposits in various rodent tissues. The dosing scheme consisted of 20 intravenous injections of 2.5 mmol gadolinium per kilogram (gadolinium-exposed group)

<https://doi.org/10.1148/radiol.2017161594>

Content code: **NR**

Radiology 2017; 285:536–545

#### Abbreviations:

GBCA = gadolinium-based contrast agent  
ICP-MS = inductively coupled plasma mass spectrometry

#### Author contributions:

Guarantors of integrity of entire study, R.J.M., J.S.M., R.K., D.F.K.; study concepts/study design or data acquisition or data analysis/interpretation, all authors; manuscript drafting or manuscript revision for important intellectual content, all authors; approval of final version of submitted manuscript, all authors; agrees to ensure any questions related to the work are appropriately resolved, all authors; literature research, R.J.M., J.S.M., D.D., M.E.J., D.L.M., R.K., L.J.E.; experimental studies, R.J.M., J.S.M., D.D., D.S., M.E.J., D.L.M., R.K., D.F.K.; statistical analysis, R.J.M.; and manuscript editing, all authors

Conflicts of interest are listed at the end of this article.

See also the editorial by Kang and the article by McDonald et al in this issue.

or saline (control group) over a 26-day period (one injection per day for 5 days and 2 days with no injections, repeated four times) by D.D. (19 years of experience) and D.S. (6 years of experience). In the gadolinium-exposed group, four GBAs were administered including gadodiamide (Omniscan; GE Healthcare, Little Chalfont, United Kingdom), gadobenate dimeglumine (MultiHance; Bracco, Milan, Italy), gadobutrol (Gadavist; Bayer, Whippany, NJ), and gadoteridol (ProHance; Bracco). This supratherapeutic dosing schedule was selected to maximize the probability of detection of gadolinium deposits among GBAs that demonstrated little, if any, T1 signal changes in prior human studies and detection probability of histopathologic findings in neural and other tissues. Injections from fresh vials of each GBA were administered into the tail vein via percutaneous vascular access under vaporized general anesthesia maintained with 4% isoflurane (Halocarbon Laboratories, River Edge, NJ). Unenhanced magnetic resonance (MR) imaging of the brain was performed in control and gadolinium-exposed rats before and after intravenous treatment. Following intravenous treatment, the rats were euthanized 7 days after the last intravenous dose of saline or GBA and fresh brain, liver, splenic, and renal tissues were harvested at necropsy for further analysis. The timing of euthanasia was chosen to minimize the effects of tissue washout and redistribution, which can confound the analysis of tissue deposition.

### MR Imaging Acquisition and Analysis

All rats in this study underwent serial MR imaging examinations of the brain that included both fast spin-echo and isotropic three-dimensional inversion recovery-prepared fast spoiled gradient-echo unenhanced T1-weighted axial sequences of the entire brain. MR imaging was performed with a 3-T Signa instrument (GE Healthcare) (R.J.M., 15 years of experience; J.P.F., 36 years of experience). Unenhanced axial T1-weighted images were obtained by using the following common imaging parameters: repetition time (msec)/echo time (msec), 400–700/10–15; matrix, 256 ×

192; and section thickness, 2 mm. MR images were analyzed by R.J.M. using OsiriX (Pixemo, Bernex, Switzerland) as previously described (3).

### Tissue Processing

Animals were euthanized with a fatal, weight-dependent injection of 100 mg/kg pentobarbital. Following sacrifice, the rat brain, liver, spleen, and kidney were extracted en bloc and hemisected during necropsy by a pathologist with expertise in animal histopathology (D.D.). For brain tissue samples, the cerebellar dentate nuclei were carefully extracted by using microdissection. Hemisected samples were placed in Trump fixative (4% paraformaldehyde + 1% glutaraldehyde in 0.1 mol/L phosphate buffer) for 24 hours prior to analysis with transmission electron microscopy. The remaining hemisected sample was initially fixed in 10% neutral-buffered formalin for 105 minutes for subsequent histopathologic examination and inductively coupled plasma mass spectrometry (ICP-MS). Histopathologic samples were sequentially immersed in alcoholic formalin (120 minutes), increasing ethanol concentrations (70%, 80%, and 95% ethanol for 30 minutes each; 100% for 55 minutes × 2), and finally in xylene (55 minutes × 2). Xylene-fixed tissues were washed in liquid paraffin (40 minutes × 3), embedded in paraffin blocks, sectioned (cerebellum = 3 μm; liver, spleen, kidney = 4 μm) by using a Leica RM 2165 microtome (Leica Biosystems, Wetzlar, Germany), floated in a water bath at 42°C, mounted on glass slides, and dried (60°C for 30 minutes). Mounted samples were stained with hematoxylin-eosin following tissue deparaffinization and hydration as previously described (15). All slides were independently reviewed by an animal pathologist (D.D.) and a board-certified pathologist (M.E.J., 10 years of experience) while blinded to contrast agent exposure.

### ICP-MS and Transmission Electron Microscopy with Electron Probe Microanalysis

Elemental gadolinium quantification of acid hydrolyzed tissue samples was performed by using ICP-MS in our

institutional College of American Pathologists-accredited heavy metals laboratory as previously described (D.L.M., 20 years of experience). Transmission electron microscopy with energy dispersive x-ray spectroscopy was performed at our institutional microscopy core facility to characterize and quantify the distribution of gadolinium deposits in these formalin-fixed tissues as previously described (T.A.C., 27 years of experience) (3,16). All tissue processing and analysis were carried out with the laboratories blinded to the tissue identity.

### Statistical Analysis

All statistical analyses were performed by R.J.M. and J.S.M. (17 years of experience) by using R (version 3.1; R Foundation for Statistical Computing, Vienna, Austria) (17). Continuous variables were presented as medians with interquartile ranges unless otherwise noted. Significant differences in relative T1 signal changes following GBA administration, relative to saline, were determined by using the nonparametric Wilcoxon signed rank test. Significant differences between GBAs in the amount of gadolinium deposited in tissues, measured by using ICP-MS, were assessed by using nonparametric Kruskal-Wallis analysis of variance tests. Post hoc Tukey-Kramer tests were performed for significant analysis of variance results to identify significant paired comparisons. Correlations between the magnitude of change in MR imaging signal intensities and ICP-MS results were assessed by using Pearson coefficient. Significance was assigned to differences of *P* values less than or equal to .05.

## Results

### Animal Population

A total of 30 healthy rats were included in this study, with six rats in each treatment group (control, gadodiamide-exposed, gadobenate dimeglumine-exposed, gadobutrol-exposed, and gadoteridol-exposed). Two rats in the gadobenate dimeglumine-exposed group acquired a tail infection during their injection series and were

ethanized according to standard Institutional Animal Care and Use Committee protocols. Three additional rats (gadodiamide-exposed, gadobenate dimeglumine-exposed, and gadobutrol-exposed) died during MR imaging due to complications from anesthesia administration. In total, 25 of 30 rats (83.3%; six control, six gadoteridol-exposed, five gadobutrol-exposed, three gadobenate dimeglumine-exposed, and five gadodiamide-exposed) completed their injection series and were euthanized for further analysis.

### Effect of GBCA Exposure on MR Imaging Signal Intensities

Qualitative changes in T1-weighted imaging within the rat dentate nucleus following multiple intravenous saline and GBCA doses are shown in Figure 1, *B* and *C*, respectively. The effects of intravenous administration of GBCA on normalized T1-weighted imaging signal changes in the dentate nucleus are shown in Figure 2. Among the GBCAs studied, gadodiamide had the greatest mean T1 signal increase and gadoteridol had the least amount of signal change. Compared with saline-injected rats that had minimal normalized changes in dentate nucleus signal intensity (<4%), gadolinium-exposed rats had significantly higher normalized T1 signal increases in their dentate nuclei compared with saline-injected control rats (Fig E1 [online]) ( $\chi^2 = 25.0$ ,  $P < .0001$ ) with significant pairwise differences between each contrast group ( $P \leq .0135$ ).

### Effect of GBCA Exposure on Neural and Nonneural Tissue Deposition

Comparisons of the amount of elemental gadolinium detected in neural tissues by ICP-MS are shown in Figure 3, *A* and the Table. In descending order, gadodiamide had the highest mean amount of gadolinium deposition in neural tissues, followed by gadobenate dimeglumine, gadobutrol, and gadoteridol (Table). Relative to control rats that had undetectable levels of elemental gadolinium, all GBCA-exposed rats had significantly elevated levels of elemental gadolinium in their dentate nuclei ranging from 0.1

**Figure 1**

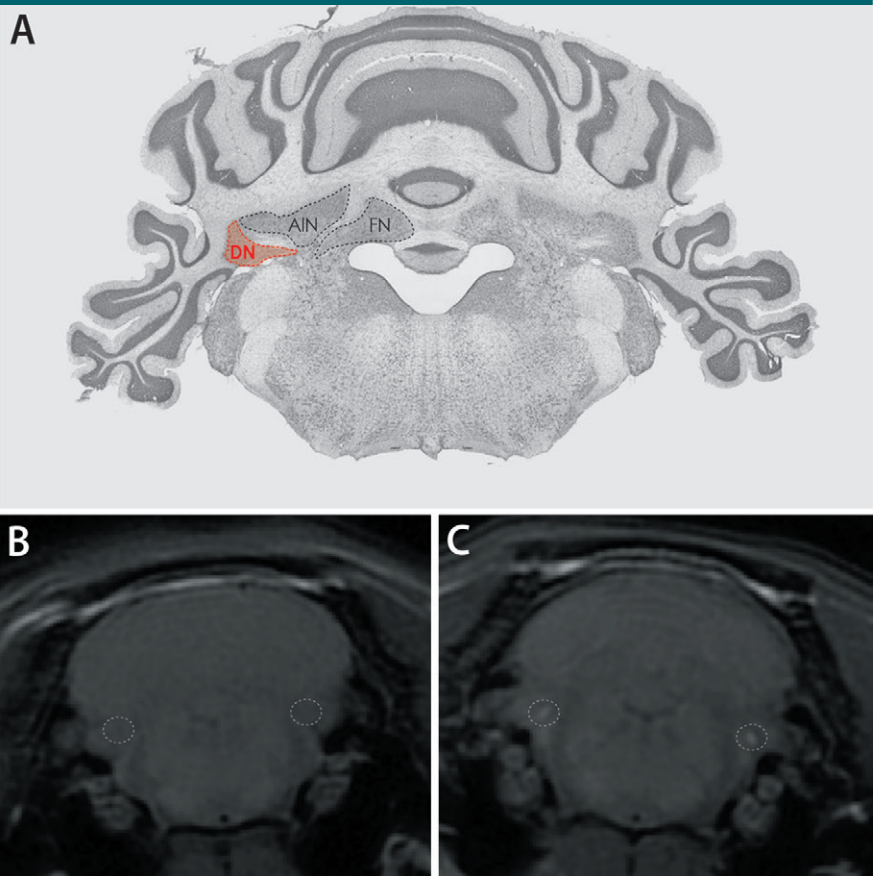


**Figure 1:** MR images show dentate nucleus. *A*, Wide-field image of hematoxylin-eosin-stained coronal slice of rat cerebellum with annotation of dentate nucleus (*DN*), anterior interpositus nucleus (*AIN*), and fastigial nucleus (*FN*). Unenhanced axial T1-weighted images through posterior fossa at level of dentate nucleus (dashed circle) are shown for, *B*, saline-exposed rat and, *C*, gadodiamide-exposed rat (total cumulative dose, 50 mmol/kg). Source.—Reference 24.

to 6.9  $\mu\text{g}$  gadolinium per gram of tissue (Fig 3, *A*) ( $H = 22.1$ ;  $P = .0002$ ). Mean elemental gadolinium concentrations within cerebellar tissues were also significantly different between GBCAs ( $P = .0459$  to  $P = .0038$ ) and demonstrated a significant positive dose-signal intensity correlation in the dentate nucleus ( $\rho = 0.93$ ;  $P < .0001$ ).

Comparison of the amount of elemental gadolinium detected in hepatic, splenic, and renal tissues by ICP-MS is shown in Figure 3, *B* and the Table. Relative to control rats, GBCA-exposed rats had significantly elevated levels of elemental gadolinium (liver:  $H = 30.0$ ,  $P < .0001$ ; spleen:  $H = 21.4$ ,  $P = .0003$ ; kidney:  $H = 23.5$ ,  $P < .0001$ ). Low levels

of elemental gadolinium in hepatic, splenic, and renal tissues of control rats were noted and likely reflect rare earth metal groundwater contamination (18,19). In these tissues, elemental gadolinium concentrations were several orders of magnitude higher in GBCA-exposed rats compared with the concentrations observed in neural tissues (liver, 8.9–511.6  $\mu\text{g}$  gadolinium per gram of tissue; spleen, 11.9–647.8  $\mu\text{g}$  gadolinium per gram of tissue; kidney, 49.5–2179.7  $\mu\text{g}$  gadolinium per gram of tissue). For each unique GBCA, median elemental gadolinium tissue concentration was significantly higher in the liver, spleen, and renal tissue compared with the dentate nucleus (gadoteridol:  $H = 23.1$ ,  $P <$

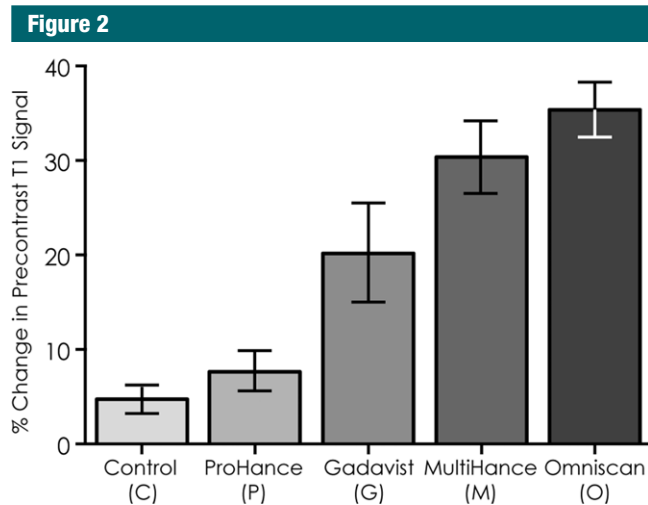


**Figure 2:** T1-weighted signal changes of MR imaging results. Quantification of change in unenhanced T1-weighted signal in rat dentate nuclei are shown for control and GBCA-exposed rats. Bars represent mean signal percentage and error bars represent standard deviation.

.0001; gadobutrol:  $H = 17.3$ ,  $P = .0006$ ; gadobenate dimeglumine:  $H = 9.7$ ,  $P = .02$ ; gadodiamide:  $H = 16.1$ ,  $P = .0011$ ).

#### Localization of Elemental Gadolinium Deposits by Using Transmission Electron Microscopy

Compared with control rats, in which elemental gadolinium deposits could not be detected by using transmission electron microscopy with energy dispersive x-ray spectroscopy within the dentate nucleus (Fig 4, A), electron dense foci were detected in the dentate tissues of all contrast agent-exposed rats (Fig 4, B–E). Despite a relative increase in electron dense foci in gadoteridol-treated rats, the characteristic x-ray spectrum of gadolinium was not detected by using this method and suggests the concentration and size of these deposits were below the detection threshold of this analytical technique. Increasing concentrations of elemental gadolinium were detected in the dentate tissues treated with gadobutrol, gadobenate dimeglumine, and gadodiamide. While a majority of these elemental gadolinium deposits were found within the endothelial wall, a smaller fraction of these electron dense elemental gadolinium deposits were identified in the

tissue interstitium (Fig E2 [online]). Densitometry performed for lower magnification views of contrast agent-exposed transmission electron microscopy samples revealed that 12%–41% of these elemental gadolinium deposits are present in the interstitium; the relationship between GBCA identity, class, and relative amount of interstitial deposition was not assessed in this study due to sample size limitations in the number of tissue samples subjected to transmission electron microscopy with energy dispersive x-ray spectroscopy.

#### Histologic Analysis

Despite evidence of elemental gadolinium deposition within neural, hepatic, and splenic tissues, no gross histologic differences were evident between control rats (Fig 5, A–C) and GBCA-exposed rats (Fig 5, E–G, gadodiamide-exposed tissue shown) on hematoxylin-eosin-stained tissue samples by using visual light microscopy. In contradistinction, the kidneys of GBCA-exposed rats demonstrated marked morphologic derangement following intravenous exposure. In the kidneys of rats exposed to gadodiamide, gadobutrol, and gadobenate dimeglumine, diffuse epithelial vacuolization of the

renal cortex was noted, but glomerular architecture was preserved (Fig 5, H, gadodiamide-exposed tissue shown). In the gadoteridol-exposed group, the histologic changes of renal injury were more extensive, with diffuse dilation and cast deposition in the renal tubules, focal tubular epithelial hyperplasia, and mononuclear inflammatory cell infiltration with peritubular inflammation and glomerular sclerosis (Fig 6, E). These histologic changes were not identified in control rats (Fig 5, D, Fig 6, A). When compared with renal tissue harvested from control rats (Fig 6, B–D), gadoteridol-exposed renal tissues demonstrated advanced ultrastructural changes that were less severe with other GBCAs and included advanced loss of normal cytoarchitecture of the proximal convoluted tubule (Fig 6, E), alterations in glomerular structure and filling of Bowman space with matrix and cellular debris (Fig 6, G), and complete loss of the outer mitochondrial membrane (Fig 6, H) that is often associated with early cellular apoptosis (20).

#### Discussion

The results of this prospective animal model study reveal a significant association between intravenous GBCA administration, chelate subtype, and the extent of deposition in neuronal, hepatic, splenic, and renal tissues. While macrocyclic agents had diminished elemental gadolinium tissue deposition compared with linear agents, significant differences in tissue concentrations were noted between macrocyclic agents. Further, all GBCAs with the exception of gadoteridol were associated with significantly elevated levels of elemental gadolinium in neural and other tissues over animals exposed to saline alone. Our current findings refute current assumptions that gadolinium deposition in neural tissues is limited to linear GBCAs.

Our current findings complement the preliminary animal model findings of Robert et al and expand on these prior studies by including a larger number of linear and macrocyclic GBCAs. Further, our study

**Mass Spectrometry Results**

Group	Dentate Nucleus	Kidney	Liver	Spleen
<b>Control (saline) group</b>				
1	0	1.9	1.9	1.7
2	0	15.5	4.4	4.7
3	0	22.8	2.8	32.5
4	0	4.5	3.4	4.4
5	0	6.2	5.1	5.1
6	0	0.7	1.9	1.8
Median	0	5.4 (1.6–17)	3.1 (1.9–4.6)	4.6 (1.8–12)
<b>Gadoteridol group</b>				
1	0	192.6	18.1	15.5
2	0	264.2	17	18.4
3	0.1	167.6	14.9	17.7
4	0.4	129.6	8.9	18.2
5	0	191.5	16	11.9
6	0.2	49.5	20.4	19.7
Median	0 (0–0.2)	168 (73–193)	16 (12–18)	18 (15–18)
<b>Gadobutrol group</b>				
1	0.8	555.2	56.7	397.3
2	6.9	657.8	47.3	176.3
3	0.9	375.2	42.7	169.4
4	2.4	322	14.6	150.3
5	1.6	689.8	45.3	200.7
Median	1.6 (0.9–4.7)	555 (349–674)	45 (29–52)	176 (160–299)
<b>Gadobenate dimeglumine group</b>				
1	3.5	1218.1	176.3	236.3
2	6.1	1288.9	101.2	118.7
3	4.7	1099.7	124.3	189.5
Median	4.7 (3.5–6.1)	1218 (1098–1289)	124 (101–176)	190 (119–236)
<b>Gadodiamide group</b>				
1	6.2	1604.6	388.4	354.1
2	7	2179.7	493.9	526.3
3	7	743.5	306.4	249.9
4	6.9	2134.1	511.6	647.8
5	6.1	2134	314.4	346.6
Median	6.9 (6.2–7.0)	2134 (1174–2157)	388 (310–503)	354 (299–587)

Note.—Data are tissue gadolinium concentrations detected with ICP-MS (in micrograms of gadolinium per gram of tissue.) Data in parentheses are the interquartile range.

provides more robust evidence of elemental gadolinium tissue deposition via ICP-MS and transmission electron microscopy compared with prior work. The larger complement of GBCAs in our study permits comparison of differences in tissue deposition potential between GBCAs with similar stability and chelate subtype. Furthermore, our study utilized more extensive methods to characterize the location and distribution of gadolinium deposits in neural tissues and

quantified tissue deposition in other organs. Such findings add to the collective knowledge of the evolving field of GBCA-mediated gadolinium tissue deposition.

Overall, our data support the initial findings of Kanda and Radbruch to the extent that linear agents have higher tissue concentrations of elemental gadolinium compared with macrocyclic agents from equivalent intravenous GBCA doses (11–14). However, juxtaposition of the deposition

propensities of several linear and macrocyclic agents facilitates comparison of observed data with predicted gadolinium tissue concentrations. One prevailing theory posits that deposition is related to chelate stability as defined by absolute and relative thermodynamic binding constants that quantify the binding strength of the gadolinium ion to the chelate ligand. For our investigation, the predicted stability of studied GBCAs in descending order is as follows: gadoteridol, gadobenate dimeglumine, gadobutrol, and gadodiamide. In agreement with these predicted trends, we report that gadoteridol and gadodiamide have the lowest and highest elemental gadolinium tissue concentrations, respectively. However, the relative tissue concentrations of gadobenate dimeglumine and gadobutrol deviate from predicted trends because we observed significantly higher deposition of gadobenate dimeglumine in all studied organs compared with gadobutrol. Such findings suggest that chelate stability alone does not define the deposition potential of these GBCAs and that other physiochemical properties such as lipophilicity and dissociation kinetics may play a role in tissue deposition (21,22). Further, the large variation in tissue deposition between macrocyclic agents expands on the existing work by Tweedle et al, Radbruch et al, Kanda et al, and others (11–14,21) and provides new data to suggest that whereas gadolinium tissue deposition is somewhat class-dependent, macrocyclic contrast agent deposition is not universally lower than linear agents, with some macrocyclic agents apparently demonstrating higher tissue gadolinium deposition than what has been previously described in skin biopsy samples and recent reports of T1-weighted signal intensity changes (23).

The observation of significantly higher gadolinium accumulation in nonneural tissues (liver, spleen, kidney), compared with neural tissues, conforms with our understanding of the capillary structure of these organs. Unlike the continuous capillary

**Figure 3**

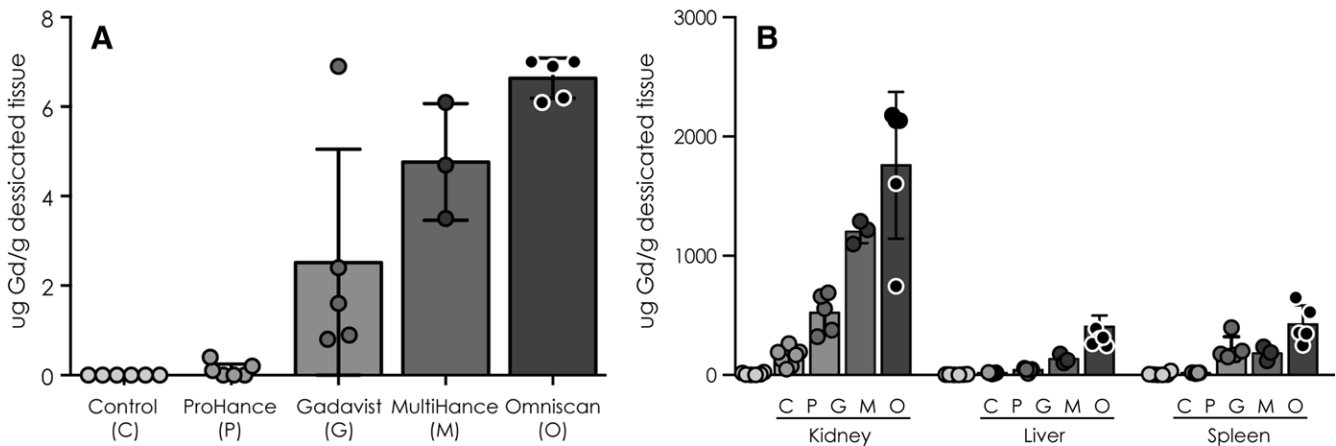


**Figure 3:** Graphs compare GBCA and elemental gadolinium tissue concentrations after intravenous GBCA exposure by using ICP-MS of rat tissues harvested at necropsy. Quantification of gadolinium ion signal detected in each rat tissue sample by using ICP-MS are plotted for control rats (injected with saline) and GBCA-exposed rats (injected with gadoteridol, gadobutrol, gadobenate dimeglumine, and gadodiamide) in, *A*, dentate nucleus and, *B*, liver, spleen, and kidney. Bars represent mean concentration, error bars represent standard deviation, and circles represent individual gadolinium concentrations derived from ICP-MS of rat tissues.

**Figure 4**

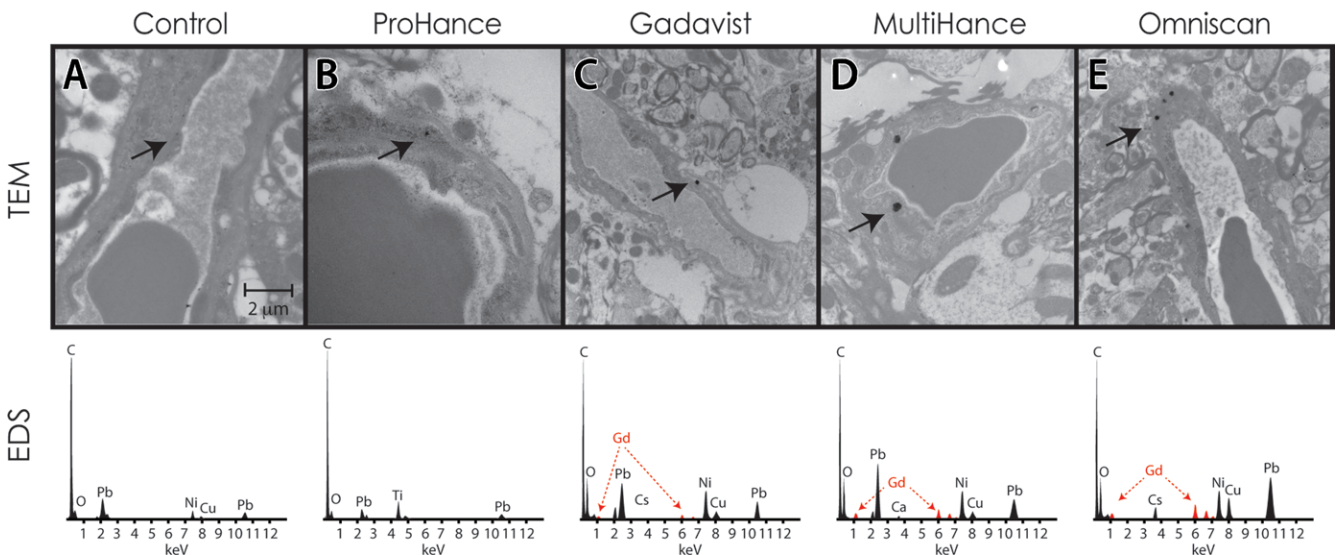


**Figure 4:** Tissue localization of gadolinium deposits. Transmission electron micrographs (0.2% lead citrate stain; original magnification,  $\times 10\,000$ ) of dentate nuclei tissue samples of, *A*, control rat and rats exposed to, *B*, gadoteridol, *C*, gadobutrol, *D*, gadobenate dimeglumine, and, *E*, gadodiamide. X-ray spectra are also shown for selected electron dense foci (arrow); gadolinium peaks in the spectra are indicated by red overlay. C = carbon, Cs = cesium, Cu = copper, Gd = gadolinium, Ni = nickel, O = oxygen, Os = osmium, Pb = lead, Ti = titanium.

structure that constitutes the blood-brain barrier in neural tissues, the hepatic and splenic tissues contain permeable, discontinuous capillaries that permit the free flow of blood products into these organs. Likewise, renal tissue capillaries are fenestrated, permitting smaller molecules to freely

exchange into the kidney parenchyma. As noted previously, the presence of gadolinium deposits within the neural interstitium challenges our understanding of the apparent impermeability of the blood-brain barrier (3). Although much of the gadolinium appears to be sequestered in deposits

that border the endothelium, possibly near tight junctions of the blood-brain barrier, the small fraction that is detected within the neural interstitium and cells suggests that this fraction of gadolinium deposits has either directly crossed or indirectly circumvented the blood-brain barrier. These

**Figure 5**

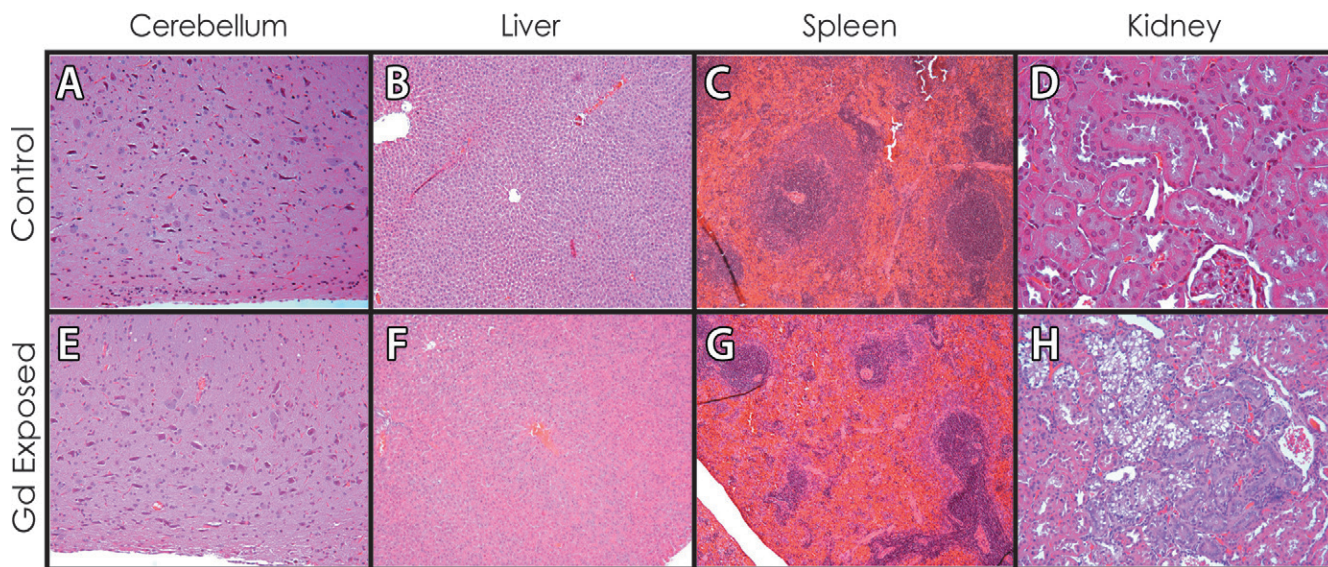


**Figure 5:** Representative photomicrographs from light microscopy (hematoxylin-eosin stain; original magnification,  $\times 100$ ) of dentate nucleus, liver, spleen, and kidney are shown for *A–D*, control group and *E–H*, gadodiamide-exposed rats. *Gd* = gadolinium.

**Figure 6**

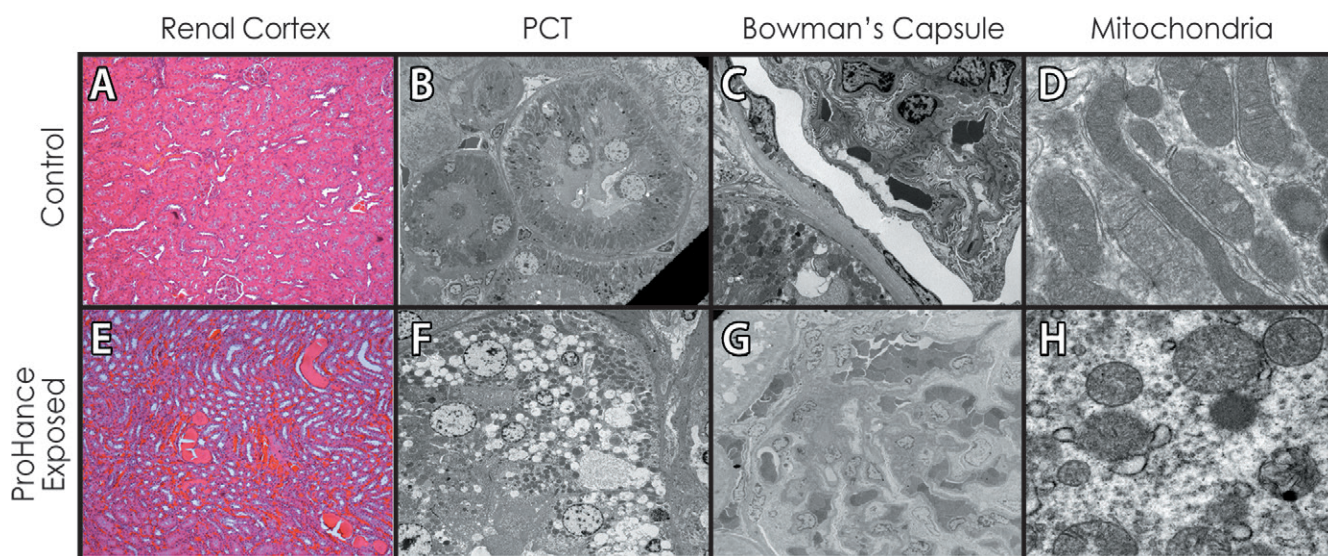


**Figure 6:** Renal histology and transmission electron microscopy results. Representative images of renal tissues of *A–D*, control and *E–H*, gadoteridol-exposed rats for *A, E*, light microscopy samples (hematoxylin-eosin stain; original magnification,  $\times 100$ ) and for *B–D* and *F–H*, transmission electron microscopy samples (hematoxylin-eosin stain; original magnification,  $\times 10\,000$ ). Transmission electron micrographs show *B, F*, proximal convoluted tubule (PCT), *C, G*, Bowman capsule of the glomerulus, and *D, H*, mitochondria.

results underscore our incomplete understanding of the mechanism of gadolinium deposition and chemical composition of these deposits. The biologic activity of these interstitial and intracellular gadolinium deposits

remains undefined, yet the considerable attention to these deposits is warranted due to their cytotoxic potential (7,8).

Similar to our previous report on human tissues (3), we did not detect

histologic abnormalities in the neural tissues of gadolinium-exposed rats, despite the elevated doses and dose frequency used in this study. By adjusting for body surface area differences between humans and rats where a

standard human dose of 0.1 mmol/kg is roughly equivalent to 0.6 mmol/kg in a rat, each animal in this study received the equivalent of a total of approximately 80 human doses (2.5 mmol/kg  $\times$  20 doses) (5). Even at these supratherapeutic doses, we were unable to identify gadolinium-mediated damage to the liver or spleen. However, we did observe renal injury in all gadolinium-exposed rats, particularly in gadoteridol-exposed rats in which there were early findings of apoptosis. Because gadoteridol had the least amount of tissue deposition, these effects are likely unrelated to the extent of deposition but do suggest small amounts of gadolinium or gadolinium chelate are entering the cell and causing renal injury. The mechanism of gadolinium-mediated renal toxicity remains undefined and merits additional investigation.

Additional study limitations persist. First, the rats in this study were subjected to higher and more frequent dosing than what humans experience in typical clinical practice. The effects of these high doses, particularly those observed in the kidneys, may be significantly attenuated or absent in human patients exposed to these agents at clinically-relevant doses and dosing schedules. Likewise, the low levels of elemental gadolinium detected following intravenous administration of macrocyclic agents at this dosing schedule is expected to be considerably lower, and possibly below the detection limit of most analytical instrumentation, by using typical human doses. Additional studies examining lower doses and less frequent administrations of GBCAs are needed. Second, the chelation state of these gadolinium deposits cannot be assessed by using the analytical methods utilized within this article; however, recent work by Birka et al using hydrophilic interaction liquid chromatography–ICP-MS has demonstrated an effective means of gadolinium tissue deposit speciation (18). Third, although no neurologic symptoms or sequelae appear to be associated with gadolinium deposition in humans or rodents, the expected cellular and physiologic effects and ultimate clinical significance

of lanthanide metal deposition within neuronal tissues is unknown and may confound our ability to identify these abnormalities.

In conclusion, our findings demonstrate that intravenous administration of high doses of GBCAs is associated with extensive multiorgan deposition that is reduced but not eliminated by use of macrocyclic GBCA chelates in lieu of linear chelates. Although no histologic changes to neural, hepatic, or splenic tissues were identified at this supratherapeutic dose, renal tissues exposed to this dosing schedule of GBCAs appear to sustain significant injury that merits additional investigation. Our findings strongly argue for future research to assess the *in vivo* stability and safety of GBCAs.

**Acknowledgments:** The authors thank Amy M. Bluhm, BS, Trace A. Christensen, BS, Jon E. Charlesworth, MA, Joel P. Felmler, PhD, and Jeffery L. Salisbury, PhD, for their technical expertise.

**Disclosures of Conflicts of Interest:** **D.J.M.** Activities related to the present article: disclosed no relevant relationships. Activities not related to the present article: institution received a grant from GE Healthcare. Other relationships: disclosed no relevant relationships. **J.S.M.** Activities related to the present article: disclosed no relevant relationships. Activities not related to the present article: institution received a grant from GE Healthcare. Other relationships: disclosed no relevant relationships. **D.D.** disclosed no relevant relationships. **D.S.** disclosed no relevant relationships. **M.E.J.** Activities related to the present article: disclosed no relevant relationships. Activities not related to the present article: has received personal fees from Bracco for participating in a symposium. Other relationships: disclosed no relevant relationships. **D.L.M.** disclosed no relevant relationships. **R.K.** disclosed no relevant relationships. **L.J.E.** disclosed no relevant relationships. **D.F.K.** Activities related to the present article: disclosed no relevant relationships. Activities not related to the present article: has received personal fees from GE Healthcare for serving on an advisory board; has received a grant from GE Healthcare. Other relationships: disclosed no relevant relationships.

## References

- Giorgi H, Ammerman J, Briffaux JP, Fretellier N, Corot C, Bourrinet P. Non-clinical safety assessment of gadoterate meglumine (Dotarem) in neonatal and juvenile rats. *Regul Toxicol Pharmacol* 2015;73(3):960–970.

- Kanda T, Fukusato T, Matsuda M, et al. Gadolinium-based contrast agent accumulates in the brain even in subjects without severe renal dysfunction: evaluation of autopsy brain specimens with inductively coupled plasma mass spectroscopy. *Radiology* 2015;276(1):228–232.
- McDonald RJ, McDonald JS, Kallmes DF, Jentoft ME, Murray DL, Thielen KR, Williamson EE, Eckel LJ. Intracranial gadolinium deposition after contrast-enhanced MR imaging. *Radiol* 2015;275(3):772–782.
- Murata N, Gonzalez-Cuyar LF, Murata K, et al. Macrocyclic and other non-group 1 gadolinium contrast agents deposit low levels of gadolinium in brain and bone tissue: preliminary results from 9 patients with normal renal function. *Invest Radiol* 2016;51(7):447–453.
- Robert P, Lehericy S, Grand S, et al. T1-weighted hypersignal in the deep cerebellar nuclei after repeated administrations of gadolinium-based contrast agents in healthy rats: difference between linear and macrocyclic agents. *Invest Radiol* 2015;50(8):473–480.
- Robert P, Violas X, Grand S, et al. Linear gadolinium-based contrast agents are associated with brain gadolinium retention in healthy rats. *Invest Radiol* 2016;51(2):73–82.
- Caillé JM, Lemanceau B, Bonnemain B. Gadolinium as a contrast agent for NMR. *AJNR Am J Neuroradiol* 1983;4(5):1041–1042.
- Tweedle MF. Physicochemical properties of gadoteridol and other magnetic resonance contrast agents. *Invest Radiol* 1992;27(Suppl 1):S2–S6.
- U.S. Food and Drug Administration. FDA drug safety communication: FDA evaluating the risk of brain deposits with repeated use of gadolinium-based contrast agents for magnetic resonance imaging (MRI). Silver Spring, Md: U.S. Food and Drug Administration, 2015.
- European Medicines Agency. EMA reviewing gadolinium contrast agents used in MRI scans. London, England: European Medicines Agency, 2016.
- Kanda T, Oba H, Toyoda K, Furui S. Macrocyclic gadolinium-based contrast agents do not cause hyperintensity in the dentate nucleus. *AJNR Am J Neuroradiol* 2016;37(5):E41.
- Kanda T, Osawa M, Oba H, et al. High signal intensity in dentate nucleus on unenhanced T1-weighted MR images: association with linear versus macrocyclic gadolinium chelate administration. *Radiology* 2015;275(3):803–809.
- Radbruch A, Weberling LD, Kieslich PJ, et al. Gadolinium retention in the dentate

- nucleus and globus pallidus is dependent on the class of contrast agent. *Radiology* 2015;275(3):783–791.
14. Radbruch A, Weberling LD, Kieslich PJ, et al. High-signal intensity in the dentate nucleus and globus pallidus on unenhanced T1-weighted images: evaluation of the macrocyclic gadolinium-based contrast agent gadobutrol. *Invest Radiol* 2015;50(12):805–810.
  15. Dai D, Ding YH, Danielson MA, et al. Modified histologic technique for processing metallic coil-bearing tissue. *AJNR Am J Neuroradiol* 2005;26(8):1932–1936.
  16. Rasband W. *ImageJ*. Bethesda, Md: U.S. National Institutes of Health, 1997–2014.
  17. R Development Core Team. *R: A language and environment for statistical computing*. Vienna, Austria: R Foundation for Statistical Computing, 2012.
  18. Birka M, Wehe CA, Hachmöller O, Sperling M, Karst U. Tracing gadolinium-based contrast agents from surface water to drinking water by means of speciation analysis. *J Chromatogr A* 2016;1440:105–111.
  19. Telgmann L, Sperling M, Karst U. Determination of gadolinium-based MRI contrast agents in biological and environmental samples: a review. *Anal Chim Acta* 2013;764:1–16.
  20. Henry-Mowatt J, Dive C, Martinou JC, James D. Role of mitochondrial membrane permeabilization in apoptosis and cancer. *Oncogene* 2004;23(16):2850–2860.
  21. Tweedle MF, Wedeking P, Kumar K. Bio-distribution of radiolabeled, formulated gadopentetate, gadoteridol, gadoterate, and gadodiamide in mice and rats. *Invest Radiol* 1995;30(6):372–380.
  22. Wedeking P, Kumar K, Tweedle MF. Dissociation of gadolinium chelates in mice: relationship to chemical characteristics. *Magn Reson Imaging* 1992;10(4):641–648.
  23. Pietsch H, Pering C, Lengsfeld P, et al. Evaluating the role of zinc in the occurrence of fibrosis of the skin: a preclinical study. *J Magn Reson Imaging* 2009;30(2):374–383.
  24. Paxinos G, Watson C. *The rat brain in stereotaxic coordinates*. 6th ed. London, England: Academic Press, 2007.